

Energy- and mass-balance comparison between Zhadang and Parlung No. 4 glaciers on the Tibetan Plateau

Meilin ZHU,^{1,4} Tandong YAO,¹ Wei YANG,¹ Fabien MAUSSION,² Eva HUINTJES,³ Shenghai LI¹

¹Key Laboratory of Tibetan Environment Changes and Land Surface Processes, Institute of Tibetan Plateau Research, Chinese Academy of Sciences, Beijing, China

²Institute for Geophysics and Meteorology, University of Innsbruck, Innsbruck, Austria

³Department of Geography, RWTH Aachen University, Aachen, Germany

⁴University of Chinese Academy of Sciences, Beijing, China

Correspondence: Wei Yang <yangww@itpcas.ac.cn>

ABSTRACT. Tibetan glaciers experience spatially heterogeneous changes, which call for further investigation of the mechanisms responsible from an energy and mass perspective. In this study, 2 year parallel observations (August 2010–July 2012) at 5665 m a.s.l. on Zhadang glacier (a subcontinental glacier) and 5202 m a.s.l. on Parlung No. 4 glacier (a maritime glacier) were used to reveal the drivers of surface energy and mass balance at these sites. Glacio-meteorological data show that air temperature and specific humidity were 1.7°C and 0.5 g kg⁻¹ lower on Zhadang glacier than on Parlung No. 4 glacier. The mass accumulation occurred primarily before the Indian summer monsoon onset on Parlung No. 4 glacier and after its onset on Zhadang glacier. Point net mass loss was 2.5 times larger on Parlung No. 4 glacier than on Zhadang glacier, mainly due to the difference in melt energy. Overall, the physical mechanisms controlling the mass and energy difference can be attributed to both the feedback role of surface albedo through different snow accumulation characteristics and longwave radiation emission of the atmosphere due to different meteorological backgrounds. Finally, a review of the few studies dealing with energy balance on the Tibetan glaciers describes the possible spatial characteristics requiring further investigation in the future on larger spatial and temporal scales.

KEYWORDS: energy balance, glacier mass balance, glacier modelling, surface mass budget, surface melt

1. INTRODUCTION

Tibetan glaciers are heterogeneous in many respects and can be categorized into different types. Shi and Liu (2000) grouped them into three types according to their continentality (maritime, subcontinental, continental). Rupper and Roe (2008) categorized them into three classes (western, eastern and northern) according to geographic differences in their spatial variability. Maussion and others (2014) defined five distinct classes of Tibetan glaciers (winter, summer and spring accumulation types and two intermediate classes) based on precipitation seasonality. All these categories are related to local climate backgrounds. Tibetan glaciers have been retreating in the past few decades as shown by numerous works, including in situ measurements and remote-sensing studies (Fujita and Ageta, 2000; Bolch and others, 2012; Yao and others, 2012; Wagnon and others, 2013). Patterns of glacier change (e.g. climatic mass balance) differ under different regimes (Jacob and others, 2012; Käab and others, 2012). However, the fundamental mechanisms controlling these spatial patterns are still disputed (Fujita and Nuimura, 2011; Scherler and others, 2011; Gardelle and others, 2012; Jacob and others, 2012; Käab and others, 2012; Yao and others, 2012), indicating that the response of Tibetan glaciers to climate change is complex due to a variety of climate settings on the Tibetan Plateau (TP) (Fujita, 2008; Rupper and Roe, 2008). Energy- and mass-balance models are a useful tool to determine the key factors affecting the climatic mass balance of glaciers, and have been successfully applied on many mountain glaciers and ice sheets around the world (Klok and

Oerlemans, 2002; Mölg and Hardy, 2004; Hock and Holmgren, 2005; Dadic and others, 2008; Mölg and others, 2008; Pellicciotti and others, 2008; Reijmer and Hock, 2008; Van den Broeke and others, 2008).

However, few detailed studies are available on glacier mass- and energy-balance processes on the TP and surrounding regions. Although some in situ point surface energy-balance measurements are available (e.g. Takahashi and others, 1989; Xie, 1994; Zhang and others, 1996; Aizen and others, 2002; Yang and others, 2011), these results are difficult to compare because of varying observation periods (e.g. ablation season or multiple years) and locations (e.g. ablation zone or accumulation zone). The characteristics of surface energy and mass balance for a few individual glaciers were analysed using an energy- and mass-balance model (e.g. Kayastha and others, 1999; Fujita and Ageta, 2000; Zhang and others, 2013). Recent studies have found that glacier energy- and mass-balance processes are closely linked with atmospheric circulation. Mölg and others (2012) quantified the impact of the Indian summer monsoon on Zhadang glacier over different monsoonal stages, and Mölg and others (2014) found that the mid-latitude westerlies are another important driver of interannual mass-balance variability on this glacier. Yang and others (2013) found that 'spring-accumulation type' glaciers, concentrated in a wedge-shaped region along the Brahmaputra River, are influenced by regional atmospheric circulations including the Indian summer monsoon, southern westerlies and the Bay of Bengal vortex. Although some experiments based on the energy- and mass-balance model have evaluated the

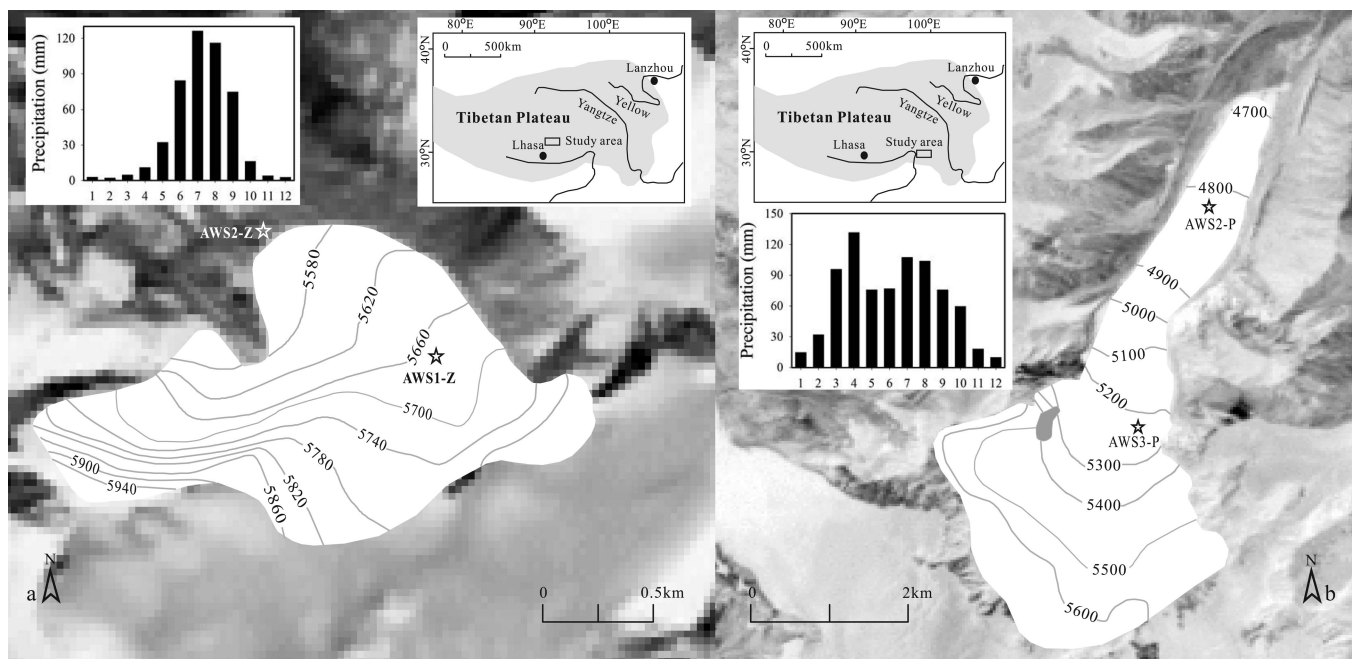


Fig. 1. Locations of Zhadang glacier (a) and Parlung No. 4 glacier (b) on the Tibetan Plateau (rectangle in the inset maps), with glacier contour maps showing locations of AWSs (stars) on both glaciers and monthly precipitation distribution (data from Damxung station nearest to Zhadang glacier and Zayu station nearest to Parlung No. 4 glacier). The glacier polygons of Zhadang and Parlung No. 4 glaciers are derived from Landsat Enhanced Thematic Mapper Plus (ETM+) 2001 and Landsat Thematic Mapper (TM) 2005 imagery, respectively.

spatial climatic sensitivity pattern of Tibetan glaciers under different climatic backgrounds (Zhang and others, 1998; Rupper and Roe, 2008; Fujita and Nuimura, 2011), most studies have focused on the relationship between a single glacier and relevant climate factors on the TP. Detailed comparisons of glacier energy- and mass-balance processes during the same periods have not been carried out in different climatic regimes.

To address this issue, we set up two automatic weather stations (AWSs) on Zhadang glacier (subcontinental glacier according to Shi and Liu, 2000) and Parlung No. 4 glacier (a maritime glacier) during the period 15 August 2010 to 25 July 2012 (Fig. 1). Both stations are located near the median elevation of each glacier and are approximately 145 and 195 m lower than the equilibrium-line altitude (ELA) for Zhadang and Parlung No. 4 glaciers, respectively. First, the relevant meteorological and energy- and mass-balance characteristics at the two AWS sites are compared. Second, the physical mechanisms that control the differences in mass loss are discussed. Third, the spatial pattern of energy fluxes on the TP and in surrounding regions is examined by reviewing recently published data on different types of glaciers.

2. DATA AND METHOD

2.1. Glacier settings

Zhadang glacier (30°28.57' N, 90°38.71' E; 2.0 km²; length 2.2 km) is located in the Nam Co basin, south TP (Fig. 1). This glacier faces north-northwest and ranges from 5515 to 6090 m a.s.l. (Shi and others, 2005). Its area decreased by 0.39 km² between 1970 and 2009 (Bolch and others, 2010). Two almost identical AWSs (AWS1-Z and AWS2-Z) were installed in the middle section (5665 m a.s.l.) and near the terminus (5580 m a.s.l.), respectively. The characteristics of the surface energy and mass balance during 2009–11 have

been analysed at both point and glacier-wide scales (Mölg and others, 2012, 2014; Zhang and others, 2013). In this study, the AWS1-Z dataset on Zhadang glacier from 15 August 2010 to 25 July 2012 was selected for comparison with the mass and energy features of Parlung No. 4 glacier.

Parlung No. 4 glacier (29°14.4' N, 96°55.2' E) lies in the Parlung–Zangbu river basin, southeast TP (Fig. 1). The glacier flows northward from an elevation of 5964 m to 4650 m, with area ~11.7 km² and length of nearly 8 km in the 1970s (Shi and others, 2005). In this region, three AWSs (AWS1-P, AWS2-P and AWS3-P) were deployed near or on Parlung No. 4 glacier. AWS1-P, located 5 km north of the glacier snout, operated on a lateral moraine at 4600 m a.s.l. Both AWS2-P (4800 m a.s.l.) and AWS3-P (5202 m a.s.l.) were located on Parlung No. 4 glacier. The summertime surface energy budget and scalar roughness length parameterization in the ablation zone at 4800 m a.s.l. have been studied by Yang and others (2011) and Guo and others (2011), respectively.

Both Zhadang and Parlung No. 4 glaciers are affected by the Indian summer monsoon in summer. However, regional precipitation seasonality shows distinct differences (Fig. 1). Zayu meteorological station (~90 km from Parlung No. 4 glacier) shows that Parlung No. 4 glacier is governed by a bimodal distribution of precipitation. Precipitation data from the Damxung meteorological station (~44 km from Zhadang glacier) show that precipitation at Zhadang glacier occurs mainly during summer.

Both AWS1-Z on Zhadang glacier and AWS3-P on Parlung No. 4 glacier recorded the following data in 10 min mean values for a nearly horizontal glacier surface: incoming solar radiation; net radiation; air temperature; relative humidity; air pressure; wind speed and direction; and subsurface ice temperature at different ice depths. Detailed specifications of all sensors are provided in Table 1. Additionally, AWS1-Z on Zhadang glacier recorded the

Table 1. Sensor information on the two AWSs used in this study with their technical specifications

Glacier	Instrument (elevation)	Sensors	Parameter*	Accuracy	
Zhadang	AWS1-Z (5665 m)	Campbell CS215	T (2.6 m)	$\pm 0.4^\circ\text{C}$	
			RH (2.6 m)	$\pm 2\%$	
		Young 05103 wind monitor	u (3.3 m)	$\pm 0.3 \text{ m s}^{-1}$	
			Campbell CS300	S_{in}	$\pm 5\%$ for daily totals
		S_{out}			
		Campbell NR-Lite	R_{net}	$\pm 5\%$ typical (10% worst case)	
			Sonic Range	SR50	0.01 m
		Apogee IRTS-P	T_s	$\pm 0.3^\circ\text{C}$	
			Campbell 107TP	T_z	$\pm 0.6^\circ\text{C}$
		Geonor T-200B	P	$\pm 0.6 \text{ mm}$	
Parlung No. 4	T-200B (5580 m) AWS3-P (5202 m)	Vaisala HMP 45C temperature and humidity probe	T (2.2 m)	$\pm 0.2^\circ\text{C}$	
			RH (2.2 m)	$\pm 2\%$	
		Young 05103 wind monitor	u (2.9 m)	$\pm 0.3 \text{ m s}^{-1}$	
			LICOR LI200X Silicon Pyranometer	S_{in}	$\pm 5\%$ for daily totals
		Sonic Range		SR50	0.01 m
		Campbell NR-Lite	R_{net} (2.7 m)	$\pm 5\%$ typical (10% worst case)	
			Geonor T-200B	P	$\pm 0.6 \text{ mm}$
		T-200B (4600 m)			

* T : air temperature; RH: relative humidity; u : wind speed; S_{in} , S_{out} , R_{net} : incoming, outgoing shortwave and net radiation; SR: glacier surface height; T_z : ice temperature; P : precipitation.

reflected solar radiation and surface temperature measured by infrared thermocouple sensor. The SR50 sonic ranging sensors were deployed near each AWS to measure the distance to the glacier surface. Two all-weather precipitation gauges (T-200B) with a hanging weighing transducer were operated close to Parlung No. 4 glacier at 4600 m a.s.l. and near Zhadang glacier at 5580 m a.s.l.

2.2. Data processing

2.2.1. Data correction

The temperature and relative humidity sensors are housed in ventilated radiation shields on Zhadang glacier and are not ventilated on Parlung No. 4 glacier. Smeets (2006) proposed a method for assessing the un aspirated temperature measurements using net shortwave radiation (S_{net}) and wind speed. With respect to the fact that S_{net} was not measured at AWS3-P (Table 1), a compromise method that uses net total radiation (R_{net}) and wind speed was adopted, and its capability was examined at AWS2-P in which both four-component radiation values were measured (Yang and others, 2011). Relative humidity (RH) data at both sites were corrected by the method of Curry and Webster (1999) when hourly air temperature was $<0^\circ\text{C}$. Corrections were applied to sonic ranger (SR50) data according to the method of Maussion and others (2011). The rain gauge undercatchment was corrected using a method suggested by Yang and others (1998) and Ma and others (2014) based on temperature and wind speed during precipitation events. The mean undercatch was estimated at 30% on Parlung No. 4 glacier and 17% on Zhadang glacier.

2.2.2. Data gap

Because of the harsh environmental conditions at high elevation, a non-negligible amount of missing data needed to be filled. The wind speed probe of AWS3-P on Parlung No. 4 glacier failed after 31 August 2010. Given the poor linear correlation between AWS1-P (moraine) and AWS2-P (glacier), we established the relationship between gridded data and wind speed available at AWS2-P on the glacier to fill in the wind speed at AWS3-P, assuming the same wind

speed over the entire glacier (Hock and Holmgren, 2005). The $0.1^\circ \times 0.1^\circ$ ITPCAS (Institute of Tibetan Plateau Research, Chinese Academy of Sciences) wind-forcing grid data (<http://dam.itpcas.ac.cn/rs/?q=data>; He and Yang, 2011) were used to fill the wind speed data gaps using the method of Giesen and others (2008). Monthly ratios were established by comparing the ITPCAS monthly wind speed in the corresponding grid with the observed values at AWS2-P. Figure 2a displays the reconstructed daily mean wind speed and the measurements at AWS2-P with a root-mean-square error (RMSE) of 2.3 m s^{-1} .

Precipitation data from T-200B were available from August 2010 to July 2012 for Zhadang glacier and from August 2010 to October 2010 and from June 2012 to October 2012 for Parlung No. 4 glacier. Yang and others (2013) showed that the reconstructed data from the ITPCAS precipitation forcing are in good agreement with the T-200B precipitation gauge records, both in cumulative number of precipitation events and cumulative precipitation amounts (Fig. 2b and c). The ITPCAS gridded precipitation from November 2010 to May 2012 was therefore used to fill in the precipitation data gap on Parlung No. 4 glacier. The RMSE of daily precipitation between the measurement and reconstructed data was 1.4 mm. Figure 2d and e display the daily precipitation near Zhadang and Parlung No. 4 glaciers, respectively.

2.3. Meteorological variables recorded by the AWSs

2.3.1. Air temperature (T) and humidity

Daily mean air temperatures at the AWS sites (AWS1-Z and AWS3-P) display an almost perfect resemblance in both daily fluctuations and annual amplitude (Fig. 3a). The mean air temperatures over the measurement periods (from 15 August 2010 to 25 July 2012) were -6.3°C on Zhadang glacier and -5.6°C on Parlung No. 4 glacier (Table 2). The mean air temperature is 1.1°C higher on Parlung No. 4 glacier in the cold season (October–May), but the temperature difference during the ablation season (June–September) is smaller on both glaciers, probably because of air cooling by the melting surface and katabatic winds. The total hours

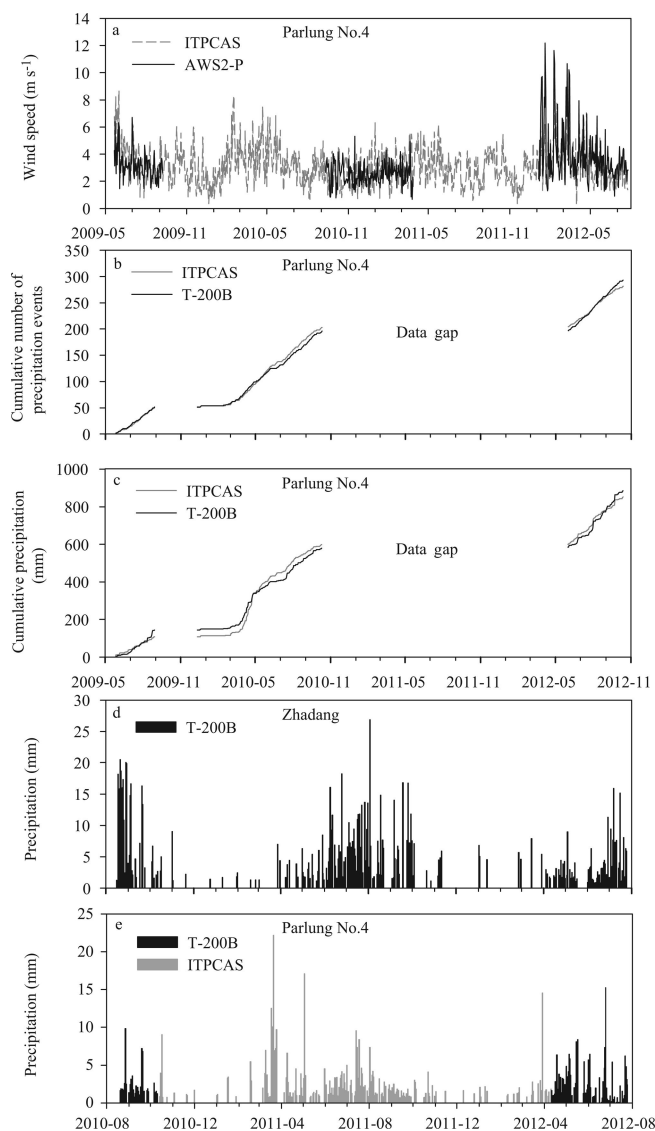


Fig. 2. (a) Comparison of measured and reconstructed wind speed at AWS2-P on Parlung No. 4 glacier and (b) cumulative numbers of precipitation events and (c) cumulative precipitation amount at Parlung No. 4 glacier between the T-200B precipitation gauge and the scaled ITPCAS precipitation data during the periods June 2009–October 2010 and June–October 2012. (d) Daily precipitation recorded by T-200B precipitation gauge near Zhadang glacier and (e) measured and reconstructed daily precipitation from ITPCAS grid data at AWS1 near Parlung No. 4 glacier. Date format is yyyy-mm.

with air temperature above 0°C were 4543 on Zhadang glacier and 5127 on Parlung No. 4 glacier.

Due to the influence of the Indian summer monsoon, the mean relative humidity is higher in summer than in winter at both sites (Fig. 3b). Relative humidity remained generally between 60% and 100%, and daily values below 50% only occurred occasionally in winter and spring. The mean relative humidity is 14% greater and the specific humidity (q) is 0.5 g kg⁻¹ higher on Parlung No. 4 glacier than on Zhadang glacier during the whole observation period, indicating a more continental climate on Zhadang glacier.

2.3.2. Wind speed (u) and wind direction (WD)

The wind speed rarely exceeded 10 m s⁻¹, and the wind direction was predominantly from the south in summer for both glaciers (Fig. 3c). Wind speed was much stronger in

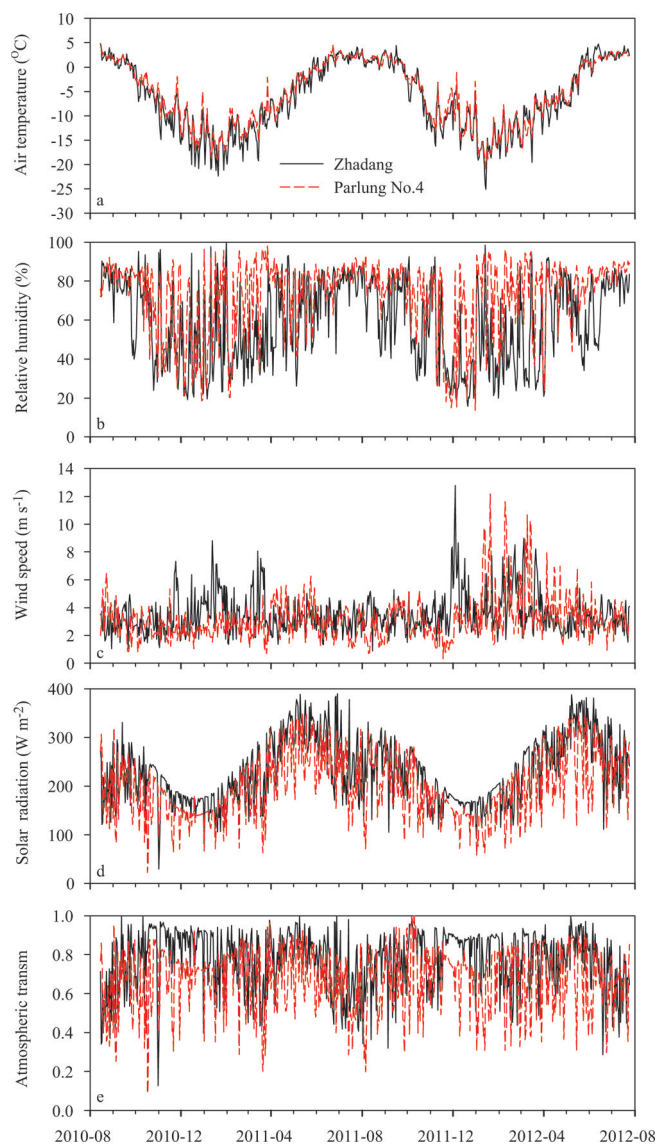


Fig. 3. Daily mean values of air temperature (a), relative humidity (b), wind speed (c), incoming shortwave radiation (d) and atmospheric transmissivity (e) at 5665 m a.s.l. on Zhadang glacier and 5202 m a.s.l. on Parlung No. 4 glacier during the observation period 15 August 2010 to 25 July 2012. The atmospheric transmissivity was calculated by the methods of Yang and others (2010). The other meteorological factors are measurement values. Date format is yyyy-mm.

winter than in summer and winds came predominantly from the northwest on Zhadang glacier and from the north on Parlung No. 4 glacier. Wind speeds are slightly higher on Parlung No. 4 glacier (Table 2). The dominant wind directions on the two glaciers are related to the local topography and local circulation (especially in the summer months) and large-scale circulation (especially in winter).

2.3.3. Incoming solar radiation (S_{in})

The mean values of S_{in} are 28 W m⁻² larger in the ablation season, and 32 W m⁻² larger in the cold season, on Zhadang glacier (Table 2; Fig. 3d). The difference in mean values of the top-of-atmosphere incoming solar radiation is neglected since the difference in latitude is only 1°. The influence of shading on S_{in} is limited, especially in the ablation season when the solar zenith angle is much smaller, so the

dominant factor determining the S_{in} difference between the two glaciers should be cloud cover (Greuell and others, 1997; Strasser and others, 2004).

To quantitatively compare the cloudy conditions in two different climatic regions, we introduce radiative transmittance, a good index for uniform cloud cover (Greuell and others, 1997). Radiative transmittance is the ratio of the measured S_{in} to the calculated clear-sky incoming shortwave radiation. Hourly clear-sky incoming shortwave radiation data are calculated using the method suggested by Yang and others (2010). Figure 3e shows that the daily mean values of atmospheric transmissivity are always higher on Zhadang glacier than on Parlung No. 4 glacier (Table 2).

2.4. The energy- and mass-balance model

The energy- and mass-balance model used in this study was first presented by Yang and others (2013) and formulas are described in the Appendix. Here we present its most important features only. The model solves for

$$M = \int \left(\frac{Q}{L_m} + \frac{H_{lat}}{L_v} + C_{en} + P_{snow} \right) dt \quad (1)$$

where M is the point mass balance (m w.e.), Q is the melt energy ($W m^{-2}$), H_{lat} is the turbulent latent heat flux (associated with ice/snow sublimation or deposition), L_m and L_v are the latent heat of ice melting ($3.34 \times 10^5 J kg^{-1}$) and evaporation/sublimation ($2.50 \times 10^6 J kg^{-1} / 2.83 \times 10^6 J kg^{-1}$), respectively, and C_{en} and P_{snow} are the accumulation owing to the refreezing of meltwater and solid precipitation (m w.e.). The refreezing amount was calculated by the model proposed by Fujita and Ageta (2000). Meltwater percolates vertically through the snowpack and refreezes where snow temperatures are below the melting point. When the snowpack is saturated with meltwater, the remaining meltwater is assumed to run off. P_{snow} is modelled by the total daily precipitation (P) and two critical

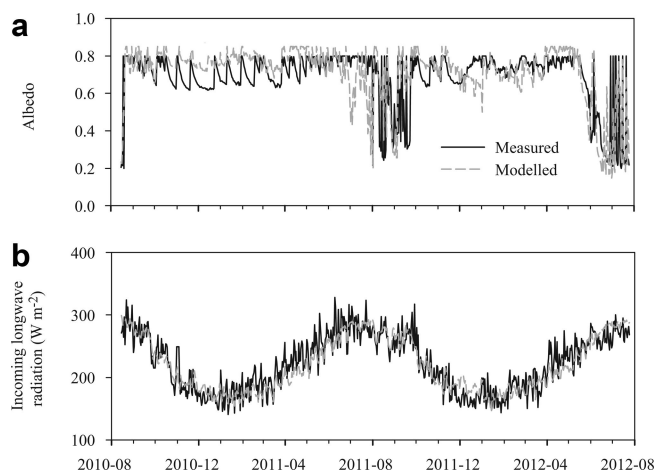


Fig. 4. Measured and modelled daily mean albedo (a) and incoming longwave radiation (b) on Zhadang glacier during the observation period 15 August 2010 to 25 July 2012. Date format is yyyy-mm.

air temperature (T) thresholds for rain (T_{rain}) and snow (T_{snow}). We used linear interpolation to separate the rain and snow from measured precipitation. Q is calculated by the surface energy-balance equation

$$Q = S_{in}(1 - \alpha) + L_{in} + L_{out} + H_{sen} + H_{lat} + QG \quad (2)$$

where S_{in} and α are the incoming shortwave radiation and albedo, and L_{in} and L_{out} are the incoming and outgoing longwave radiation. Albedo and L_{in} were optimized by AWS2-P on Parlung No. 4 glacier and AWS1-Z on Zhadang glacier (Fig. 4). The RMSE between the modelled and measured values is 0.11 and $19 W m^{-2}$ for albedo and L_{in} , respectively. H_{sen} and H_{lat} are the sensible and latent heat fluxes and QG is the subsurface heat flux. Net longwave radiation is written as L_{net} . R_{net} is the sum of S_{net} and L_{net} . All

Table 2. Mean values of meteorological variables and energy fluxes ($W m^{-2}$) during different periods between 15 August 2010 and 25 July 2012 on Zhadang and Parlung No. 4 glaciers

Parameter	Zhadang			Parlung No. 4		
	Cold season	Ablation season	Mean	Cold season	Ablation season	Mean
T ($^{\circ}C$)	-10	1.7	-6.3	-8.9	1.7	-5.6
u ($m s^{-1}$)	3.7	3.2	3.5	3.2	2.9	3.1
RH (%)	52	75	59	68	83	73
q ($g kg^{-1}$)	1.99	6.33	3.36	2.62	6.55	3.86
τ	0.81	0.7	0.77	0.69	0.62	0.67
S_{in} ($W m^{-2}$)	221	250	230	189	222	200
Albedo	0.73	0.6	0.68	0.69	0.45	0.61
S_{out} ($W m^{-2}$)	161	149	157	131	101	122
S_{net} ($W m^{-2}$)	60	101	73	58	121	78
L_{in} ($W m^{-2}$)	196	274	221	206	294	234
L_{out} ($W m^{-2}$)	260	314	277	268	315	283
L_{net} ($W m^{-2}$)	-64	-40	-56	-62	-21	-49
R_{net} ($W m^{-2}$)	-4	61	17	-3	100	29
H_{sen} ($W m^{-2}$)	16	8	13	17	14	16
H_{lat} ($W m^{-2}$)	-12	-10	-11	-11	-6	-10
G ($W m^{-2}$)	4	0	2	2	0	2
QPS ($W m^{-2}$)	-4	-13	-7	-5	-13	-7
Q ($W m^{-2}$)	0	46	14	0	95	30
Snowfall (m w.e.)	0.28	0.83	1.1	0.97	0.21	1.18
Total precipitation (m w.e.)	0.28	0.97	1.25	1	0.88	1.88

Note: Cold season is defined as October–May, and ablation season as June–September. Bold variables are measured values.

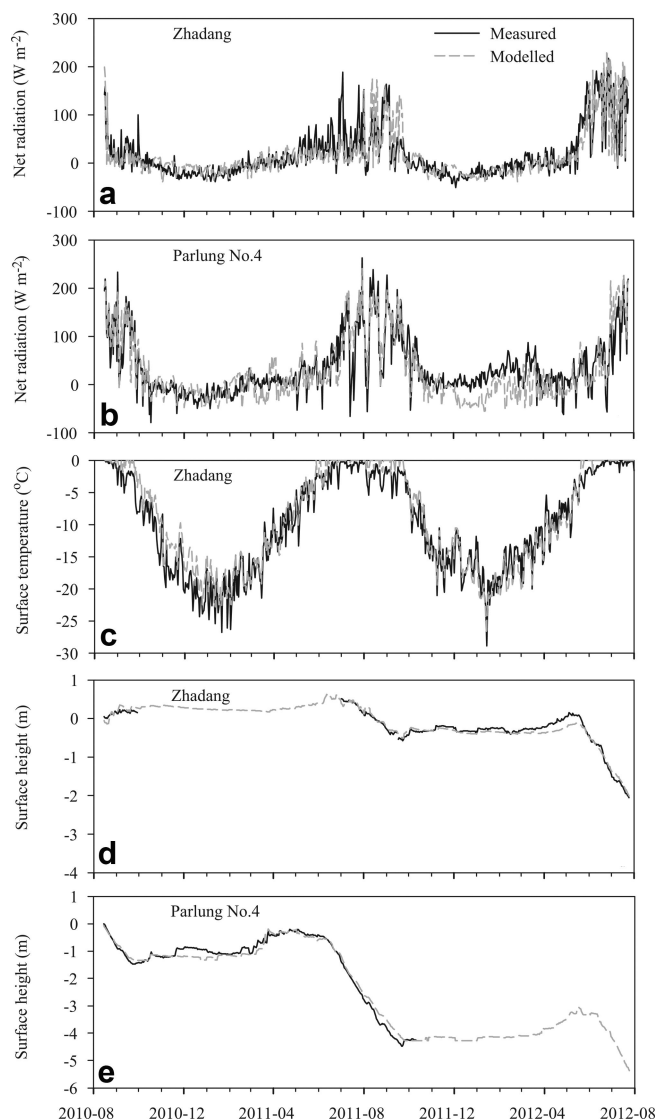


Fig. 5. (a, b) Measured and modelled daily mean net radiation on Zhadang glacier (a) and Parlung No. 4 glacier (b) during the observation period 15 August 2010 to 25 July 2012. (c) Comparison between measured and modelled daily mean surface temperature at the AWS site on Zhadang glacier. (d, e) Evolution of surface heights measured by SR50 sensor (black), compared with the modelled curves (grey) at the AWS sites on Zhadang glacier (d) and Parlung No. 4 glacier (e). Date format is yyyy-mm.

fluxes are defined as positive when directed towards the surface. Heat supplied by rain is neglected in this study. The subsurface melt has not been calculated in the model, as in previous works (e.g. Fujita and others, 2000; Hock and Holmgren, 2005; Oerlemans and others, 2009). The units of energy-balance components are W m^{-2} . The parameters of the model are listed in Table 5 in the Appendix.

A set of observed daily data (air temperature, relative humidity, wind speed, precipitation and incoming shortwave radiation) from measurement periods was used as input data to run the energy- and mass-balance model. The initial and boundary conditions are set as follows. The initial snow thickness was set to zero on both sites. The densities of fresh snowfall and ice are 200 and 900 kg m^{-3} , respectively, on both glaciers. The snowpack density will change with the refreezing of capillary water. In the model, the ice temperature at the lowest boundary was assumed to remain stable. The initial ice temperature profile was generated by

continuously running the model over the measurement period until the 10 m temperature (-3.5°C) on Parlung No. 4 glacier and the 8 m temperature (-5.5°C) on Zhadang glacier were stable within 0.01°C .

3. RESULTS

3.1. Model performance and parameter sensitivity

3.1.1. Model performance

Measured R_{net} , surface temperature (T_s) and surface height were used to evaluate the model results. Figure 5a and b show the modelled versus observed daily average R_{net} for two AWS sites. The bias between measured and modelled R_{net} is 1 and 5 W m^{-2} for Zhadang glacier and Parlung No. 4 glacier, respectively, during the observation periods. The RMSE between modelled and observed R_{net} is 29 and 34 W m^{-2} , and the correlation coefficient is 0.84 and 0.85 , for Zhadang and Parlung No. 4 glaciers, respectively, during the observation periods. T_s was measured by AWS1-Z on Zhadang glacier (Fig. 5c). The overall agreement is good, although the surface temperatures are somewhat overestimated in the snow/ice transition period. The RMSE between modelled and observed T_s is 2.1°C , with a correlation coefficient of 0.96 . Figure 5d and e show that the model reproduces the measured surface heights quite well. The RMSE between daily measured and modelled glacier surface heights (SR) is 0.11 and 0.18 m on Zhadang and Parlung No. 4 glaciers, respectively, over the measurement period.

3.1.2. Parameter sensitivity and uncertainty

Analysis of parameter sensitivity can be used to test the reliability of the mass components and to indicate which parameters are more influential in determining glacier mass-balance fluctuations. Sensitivity to individual parameters was investigated using the method of Anslow and others (2008). One parameter is varied by 5% intervals around the optimum values spanning a range of $\pm 30\%$, and other parameters were held unchanged. Thirteen resulting values of the model mass-balance output were fitted using second-order polynomials. The slope of the second-order polynomials near the origin is used as an indicator of the sensitivity of the model to a given parameter (Anslow and others, 2008; Heynen and others, 2013).

Figure 6 shows the magnitude of the calculated sensitivity for the parameters. For both glaciers, the most sensitive of the parameters are related to those in the albedo model (e.g. $a_{\text{freshsnow}}$ and a_{firn}) and variations in C_1 and C_2 in the L_{in} model. The sensitivity to the parameterization of albedo is high because shortwave radiation provides up to 60% of the melt energy on both glaciers. The higher mass-balance sensitivity to variations in the C_1 and C_2 of the L_{in} model shows that L_{in} has a great influence on the ablation rates. Indeed, L_{in} is an important energy gain for the glacier melt, and the daily L_{in} is larger than S_{in} in the ablation season on both glaciers (Table 2). The parameters of albedo and L_{in} can be carefully calibrated using measured values, which can reduce the uncertainty of the model. For the transfer coefficient of the turbulent heat flux calculation, the lower sensitivity is a result of the lower sum of H_{sen} and H_{lat} on both glaciers. The parameters related to snowfall, i.e. the threshold temperature (T_{rain}), affect the mass balance by changing the accumulation and albedo, and the ratio of penetrating S_{net} affects the energy for melt.

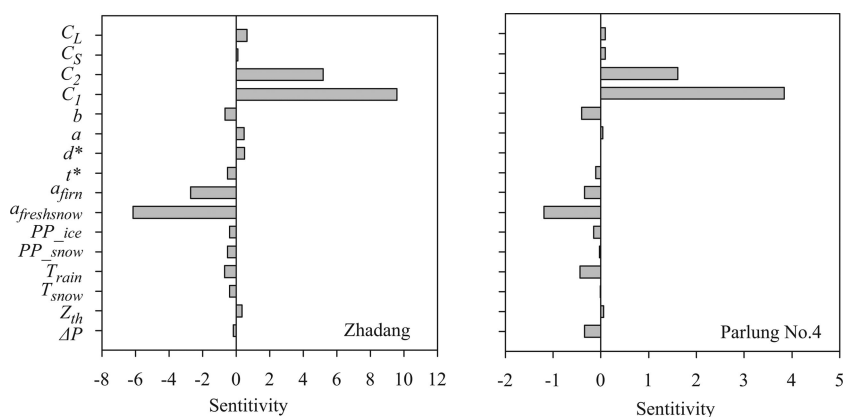


Fig. 6. Sensitivity of parameters for Zhadang and Parlung No. 4 glaciers during the observation period 15 August 2010 to 25 July 2012. Sensitivity is given as change in total mass balance per parameter change (dimensionless; from fig. 3 of Heynen and others, 2013).

In addition, using Monte Carlo methods it is possible to evaluate the uncertainty in energy- and mass-balance model output to random errors in the parameters (Anslow and others, 2008; Machguth and others, 2008). We analysed a suite of 1000 model runs to evaluate the distribution of simulated mass balance over a range of parameter values (randomly by $\pm 5\%$). We did not take into account the parameters for albedo and L_{in} on Zhadang glacier and parameters for L_{in} on Parlung No. 4 glacier because they were calibrated by the measurements. The standard deviations of 1000 runs are 0.08 m w.e. on Zhadang glacier and 0.34 m w.e. on Parlung No. 4 glacier, and both are $<10\%$ of the total mass balance by control model during the observation period.

3.2. Energy fluxes on the two glaciers

The surface energy components on two glaciers are shown in Figure 7. The melt energy is 2.1 times larger on Parlung No. 4 glacier than on Zhadang glacier during the whole observation period, and melt mainly occurs in the ablation season (June–September). S_{net} is, on average, 20 W m^{-2} larger on Parlung No. 4 glacier (Table 2) in the ablation season, as a result of different albedos of Zhadang and Parlung No. 4 glaciers. The mean surface albedo during the ablation season is ~ 0.15 higher on Zhadang glacier than on Parlung No. 4 glacier. In addition, L_{net} is 19 W m^{-2} less negative on Parlung No. 4 glacier than on Zhadang glacier in the ablation season (Fig. 7; Table 2). L_{in} is 20 W m^{-2}

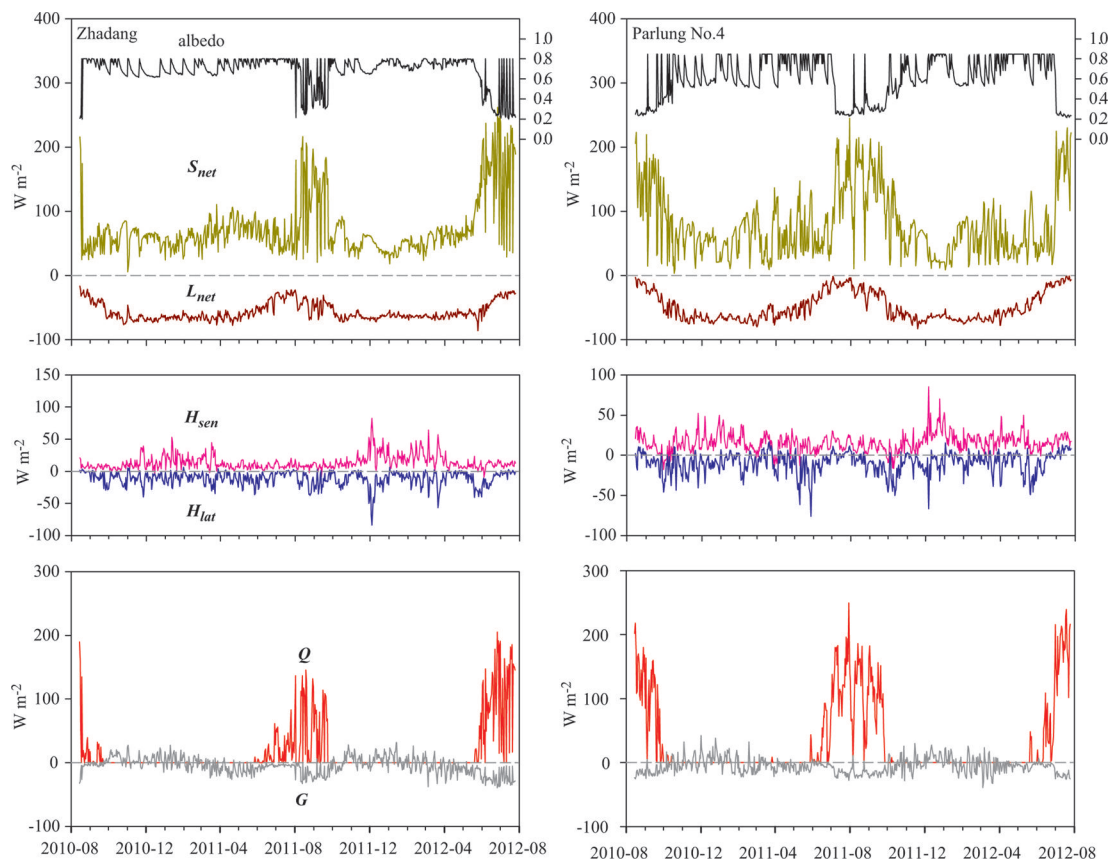


Fig. 7. Modelled daily mean surface energy fluxes on Zhadang and Parlung No. 4 glaciers during the observation period 15 August 2010 to 25 July 2012. Date format is yyyy-mm.

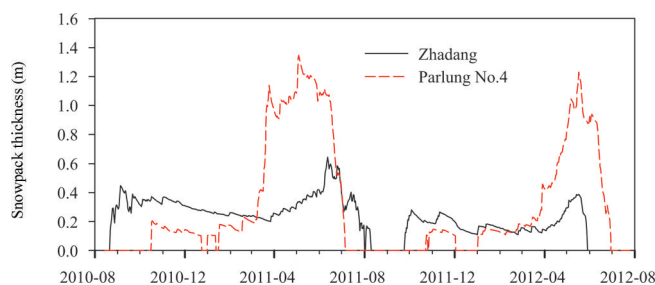


Fig. 8. Modelled daily values of snowpack thickness at the AWS sites on Zhadang and Parlung No. 4 glaciers during the observation period 15 August 2010 to 25 July 2012. Date format is yyyy-mm.

higher on Parlung No. 4 glacier than on Zhadang glacier in the ablation season due to higher temperature, humidity and cloudiness, but L_{out} was nearly equal on both glaciers. H_{sen} is 6 W m^{-2} larger on Parlung No. 4 glacier than on Zhadang glacier in the ablation season due to higher air temperatures (Table 2). H_{lat} is 4 W m^{-2} larger on Parlung No. 4 glacier in the ablation season because of a lower or reversed specific humidity gradient during a short period in summer, which means that condensation can occur (Fig. 7). The ground heat flux is small compared with the other energy fluxes (Fig. 7; Table 2). The average values of G and QPS in the ablation season are almost the same on both glaciers.

3.3. Mass-balance characteristics of the two glaciers

The glacier mass balance consists of surface melt, sublimation/evaporation, refreezing and snowfall. The point mass balance at the AWS site was -4.5 m w.e. on Parlung No. 4 glacier, nearly 2.5 times larger than for Zhadang glacier, during the period 15 August–25 July 2012 (Table 3). Surface melt dominated the glacier mass loss, with values of 2.85 m w.e. on Zhadang glacier and 5.63 m w.e. on Parlung No. 4 glacier. Mass loss through sublimation/evaporation was minor compared to surface melt, and sublimation/evaporation was similar on both glaciers ($\sim 0.25 \text{ m w.e.}$ on Zhadang glacier and 0.21 m w.e. on Parlung No. 4 glacier). During the cold season, sublimation is the most important factor for mass loss on both glaciers.

Mass gain is primarily due to solid precipitation, with a contribution of 1.18 m w.e. on Parlung No. 4 glacier and 1.1 m w.e. on Zhadang glacier during the observation periods (Table 3). Snow reaches its maximum thickness of 1.32 m at AWS3-P on Parlung No. 4 glacier in spring, but hardly any snow accumulates during summer at the same site (Fig. 8). On Zhadang glacier, the maximum snow-cover height reaches 0.64 m at the Indian summer monsoon onset (25 May–24 June; Mölg and others, 2014), and frequent snowfall occurs in the ablation season (Fig. 8). In addition, we modelled a certain amount of meltwater that refroze into the snowpack, an important englacial mass storage on both glaciers. The refreezing amounts were similar on both glaciers (0.18 m w.e. on Zhadang glacier and 0.16 m w.e. on Parlung No. 4 glacier; Table 3).

4. DISCUSSION

4.1. Representation of energy- and mass-balance comparison by two AWSs

The glacier equilibrium line is generally suitable for study of the different energy-balance and mass-balance

Table 3. Point-scale mass-balance components and surface characteristics between Zhadang and Parlung No. 4 glaciers for the observation period 15 August 2010 to 25 July 2012

	Zhadang	Parlung No. 4
Mass balance (m w.e.)	-1.82	-4.5
Melting (m w.e.)	-2.85	-5.63
Sublimation/evaporation (m w.e.)	-0.25	-0.21
Solid precipitation (m w.e.)	1.1	1.18
Refreezing (m w.e.)	0.18	0.16
Total precipitation (m w.e.)	1.15	1.92
Liquid precipitation (m w.e.)	0.16	0.77
Number of days without snowpack	113	243
Number of days with surface melting	174	204

characteristics. It is directly related to regional climate and provides a common measure location whereby changes can be compared directly (Rupper and Roe, 2008). Measured ELAs were available for both glaciers during the 2005/06 and 2006/07 balance years (Yao and others, 2010; Yu and others, 2013). The elevation differences between the mean ELA (2 year average) and AWSs are 145 and 195 m on Zhadang and Parlung No. 4 glaciers, respectively. However, we note that the ELAs have obvious interannual fluctuations on Zhadang and Parlung No. 4 glaciers. A surrogate way to represent the balanced budget ELA is the mid-range altitude (Evans and Cox, 2005; Braithwaite and Raper, 2009). The differences between the AWS sites and the mid-range altitude are 107 m and 137 m on Parlung No. 4 and Zhadang glaciers, respectively. This comparison of two AWS datasets may be considered an indicator of the meteorology and energy- and mass-balance differences.

4.2. Mechanism controlling the mass- and energy-balance difference between the two glaciers

Although both glaciers are influenced by the Indian summer monsoon during the ablation season, the point net mass loss was much larger on Parlung No. 4 glacier than on Zhadang glacier. In examining the temporal differences between each mass-balance component (Fig. 9a), it is clear that both solid precipitation and melt show large seasonal differences.

As shown in Figure 9a, snowfall is larger on Zhadang glacier than on Parlung No. 4 glacier during summer (June–August), but less than on Parlung No. 4 glacier during spring (March–May). Most glaciers on the TP are ‘summer-accumulation type’, where maximum surface ablation and mass accumulation occur simultaneously in the summer, after the Indian summer monsoon (Ageta and Higuchi, 1984; Fujita, 2008; Maussion and others, 2014). Figure 8 and Table 2 show that snowfall events on Zhadang glacier primarily occur from June to September. In contrast, the maximum surface mass accumulation for glaciers on the southeastern TP occurs before the Indian summer monsoon onset. Snowfall and snow accumulation during March–May on Parlung No. 4 glacier is obvious from Figure 8 and Table 2, indicating that different accumulation stages (summer for Zhadang vs spring for Parlung No. 4 glacier) contribute to seasonal differences in the snowfall supply.

Figure 9a also illustrates distinct seasonal mass melt. Figure 9b shows that the dominant factor controlling such differences is net shortwave radiation followed by net long-wave radiation. Since both summer and annual incoming

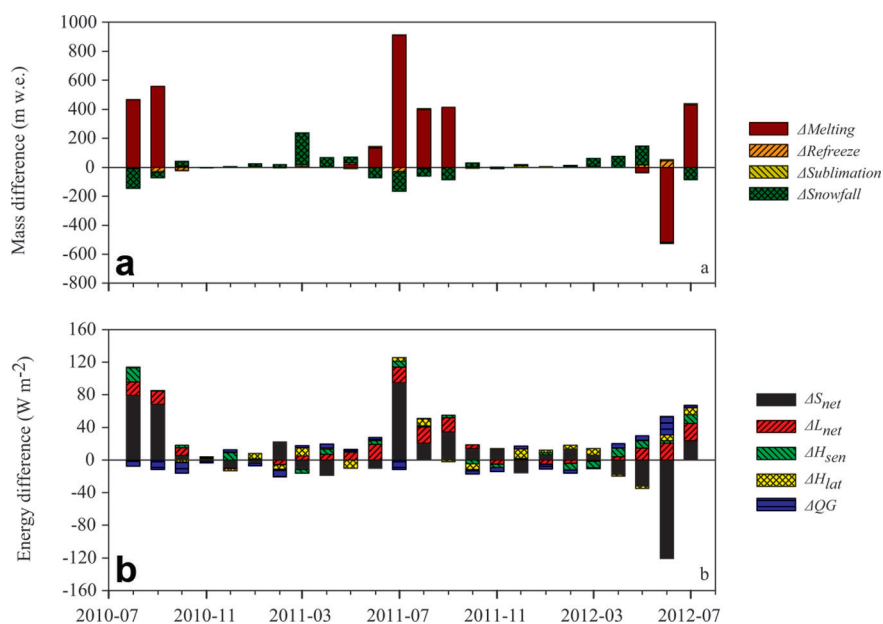


Fig. 9. Monthly differences of mass balance (a) and energy balance (b) between Parlung No. 4 and Zhadang glaciers. Note that the individual mass difference is defined as positive (negative) when the absolute value is larger (smaller) on Parlung No. 4 glacier. Date format is yyyy-mm.

solar radiations are larger on Zhadang glacier due to less cloud cover (Table 2), higher surface albedo may be responsible for this lower net shortwave radiation. The most striking differences occur in July–September, when Zhadang glacier has more frequent and a greater amount of snowfall than Parlung No. 4 glacier (Figs 8 and 9). Due to the surface snow albedo feedback mechanism (Oerlemans and others, 2009), more solar radiation will be absorbed for snowmelt due to a lower albedo, which in turn accelerates disappearance of the snowpack and sustains a lower albedo.

In addition to surface albedo, a secondary but important factor for energy difference between the two glaciers is L_{in} (Fig. 9b; Table 2). For example, during the 2011 ablation season, the mean values of L_{in} were $\sim 21 W m^{-2}$ larger on Parlung No. 4 glacier and displayed a weak seasonal pattern. The value of L_{in} depends on the temperature and humidity of the atmosphere and on cloud cover (Sicart and others, 2010). As shown in Table 2 and Figure 3, Zhadang glacier lies under a relatively cold-arid and cloudless environment, whereas Parlung No. 4 glacier exists in a warm-humid and cloudy climate. The longwave radiation emission capacity of the atmosphere is stronger on glaciers on the southeastern TP.

4.3. Energy-balance comparison to other glaciers on the TP

To compare the surface energy fluxes with values from other glaciers, we collected published energy flux data obtained from different glaciers on the TP (Table 4). The criteria for these data are that the reported values consist mostly of averages in the ablation zone over the ablation season. It should be kept in mind that these comparisons are altered by the different empirical methods for turbulent heat flux calculation, different meteorological conditions in different observational years, and the accuracy of instruments in different studies. The objective of our comparison is to detect possible spatial characteristics of energy balances on different types of glaciers under different climatic conditions.

From the energy consumption perspective, energy losses below or at the ELA on most maritime and subcontinental glaciers appear to be dominated by surface melting, whereas the energy for surface sublimation (H_{lat}) appeared to increase on the continental glaciers (Xiao Dongkemadi glacier and Chongce ice cap). This pattern is consistent with Rupper and Roe's (2008) large-scale theoretical energy- and mass-balance model, showing ablation at the ELA is dominated by sublimation in regions where precipitation is low, but controlled by melting in regions where precipitation is high. Such differences in energy consumption between maritime/subcontinental and continental glaciers indicate a spatial variability in sensitivity to climate change on different glaciers (Fujita, 2008; Rupper and Roe, 2008).

From the energy supply perspective, net radiation is the largest source of incoming energy on most Tibetan glaciers, followed by sensible heat flux. The percentage contribution of net radiation to surface energy supply ranges from 70% to 85% on most maritime and subcontinental glaciers (except Guxiang No. 3 glacier), but this percentage decreases on the continental glaciers (50% for Xiao Dongkemadi glacier and 67% for Chongce ice cap).

Finally, energy for surface melting on different types of glaciers seems to be related to their geographical climate conditions. We take Parlung No. 4, Qiyi, Keqicar Baxi and Xiao Dongkemadi glaciers as examples for comparison. The observational elevation of Parlung No. 4 glacier (4800 m a.s.l.) is higher than that of the other glaciers. However, the melting energy on this glacier is approximately two to three times larger than that of the other glaciers. This warm-wet climatic combination provides additional L_{in} and turbulent heat flux for glacier melt, and the higher air temperature may lead to less accumulation and lower albedo on the glacier due to reduced snowfall. However, we assume that the available energy experiments represent the mean condition of each glacier, without considering the annual variation of energy components. Therefore, we acknowledge that the quantification of the

Table 4. Comparison of mean energy fluxes ($W m^{-2}$) between different types of glaciers on the Tibetan Plateau for the ablation season (note different lengths of periods) and at the point scale

Glacier type*	Glacier	Lat. °N	Long. °E	Elevation m a.s.l.	ELA	Period	R_{net}	H_{sen}	H_{lat}	QC	Q	Source
Maritime	Parlung No. 4	29.2	96.8	4800	5397 ^a	May–Sep 2009	149	28	–1	–1	175	Yang and others (2011)
	Parlung No. 4	29.2	96.8	5202	5397 ^a	May–Sep 2011	84	12	–11	–12	73	This study
	Guxiang No.3	29.9	95.4	4400	–	Jul–Aug 1965	148.1	62.5	18.5	–	229.2	Wang and others (1982)
Subcontinental	Zhadang	30.4	90.6	5655	5810 ^b	May–Sep 2011	39	8	–11	–11	25	This study
	Laohugou No.12	39.4	96.4	5040	4830 ^c	Jun–Sep 2006	27.3	10.3	–11.9	–7.6	18.2	Sun and others (2012)
	Qiyi	39.5	97.7	4473	4773 ^d	Jul–Oct 2007	63.3	14.2	–6.1	–15.5	55.8	Jiang and others (2010)
	Keqicar Baxi	41.8	80.05	4200	4631 ^e	Jun–Sep 2005	63.3	14.4	–23	–	54	Li and others (2007)
	Ürümqi glacier No.1	43.1	86.8	3910	4013 ^f	Jun–Aug 1986–90	73	13	–5	–	81	Kang and Ohmura (1994)
Extremely continental	Xiao Dongkemadi	33	92	5600	5545 ^g	Sep 1989 to Sep 1992	44	44	–64.3	–1.2	21.4	Zhang and others (1996)
	Chongce ice cap	35.2	81.01	5850	5930 ^h	Jul–Aug 1987	35.9	17.4	–39.4	–	13.9	Takahashi and others (1989)

*Classified according to Shi and Liu (2000).

^aYao and others (2010); ^bYu and others (2013); ^cKang and Ding (1981); ^dWang and others (2010); ^eZhang and Liu (2006); ^fDong and others (2012); ^gPu and others (1995); ^hAgeta and others (1989).

relationship between melting energy and geographical conditions requires further work, including additional observations during the same observation periods and using the same experimental procedures.

5. CONCLUSIONS

Based on 2 years of glacio-meteorological data observed from 15 August 2010 to 25 July 2012 on Zhadang and Parlung No. 4 glaciers, we studied the point-scale energy- and mass-balance differences between subcontinental and maritime glaciers of the TP using a physical energy and mass-balance model. Meteorological conditions reveal a maritime climate on Parlung No. 4 glacier, with higher air temperature, higher humidity and more frequent cloud cover than the relatively cold-dry climate on Zhadang glacier. The mass-balance comparison shows that mass accumulation on Parlung No. 4 glacier occurred mainly before the Indian summer monsoon onset, but the maximum mass accumulation for Zhadang glacier occurred after the Indian summer monsoon. On Parlung No. 4 glacier, total net mass loss at the AWS site was 4.5 m w.e., nearly 2.5 times higher than for Zhadang glacier. The largest difference lies in the amount of melt, with values of 2.85 m w.e. on Zhadang glacier and 5.63 m w.e. on Parlung No. 4 glacier. Different albedos and different longwave radiation emission of the atmosphere under these two climatic environments determine the mass loss difference between the two glaciers. Finally, a tentative analysis of the spatial characteristics of glacier energy fluxes on the TP and in the surrounding regions found possible energy-balance patterns under different climatic conditions. But it elucidated the general problems of data availability and consistency that hinder the quantitative comparison of glacier responses under various climatic conditions. In our study we used a consistent

modelling system on two glaciers during a parallel time period, which is a step forward. Future studies should focus on distributed modelling on larger spatial and temporal scales.

ACKNOWLEDGEMENTS

We acknowledge the staff at the Nam Co Monitoring and Research Station for Multisphere Interactions, Institute of Tibetan Research, Chinese Academy of Sciences (CAS), for help in the field. We thank four anonymous reviewers and the editor, Thomas Mölg, for valuable insights that greatly strengthened the manuscript. We thank the National Climate Center, China Meteorological Administration, for providing the climate data used herein. This study was jointly funded by the National Natural Science Foundation of China (grant 41190081), the Strategic Priority Research Program (B) of CAS (grant XDB03030208) and the National Natural Science Foundation of China (NSFC) (grants 41371085 and 41201058). F.M. and E.H. acknowledge support from the German Federal Ministry of Education and Research (BMBF) Programme 'Central Asia – Monsoon Dynamics and Geo-Ecosystems' (CAME) within the WET project ('Variability and Trends in Water Balance Components of Benchmark Drainage Basins on the Tibetan Plateau') under the code 03G0804A and 03G0804E, and from the German Research Foundation (DFG) Priority Programme 1372, 'Tibetan Plateau: Formation–Climate–Ecosystems', within the DynRG-TiP ('Dynamic Response of Glaciers on the Tibetan Plateau to Climate Change') project under the codes SCHE 750/4-1, SCHE750/4-2, SCHE 750/4-3 and SCHN 680/3-1, SCHN 680/3-2, SCHN 680/3-3. F.M. acknowledges further support from the Austrian Science Fund (FWF project P22443-N21).

REFERENCES

- Ageta Y and Higuchi K (1984) Estimation of mass balance components of a summer-accumulation type glacier in the Nepal Himalaya. *Geogr. Ann. A.*, **66**(3), 249–255 (doi:10.2307/520698)
- Ageta Y, Zhang W and Nakawo M (1989) Mass balance studies on Chongce Ice Cap in the west Kunlun Mountains. *Bull. Glacier Res.*, **7**, 37–43
- Aizen V, Aizen E and Nikitin S (2002) Glacier regime on the northern slope of the Himalaya (Xixibangma glaciers). *Quat. Int.*, **97**, 27–39 (doi:10.1016/S1040-6182(02)00049-6)
- Anslow FS, Hostetler S, Bidlake WR and Clark PU (2008) Distributed energy balance modeling of South Cascade Glacier, Washington and assessment of model uncertainty. *J. Geophys. Res.*, **113**(F2), F02019 (doi: 10.1029/2007JF000850)
- Bolch T and 7 others (2010) A glacier inventory for the western Nyainqentanglha Range and the Nam Co Basin, Tibet, and glacier changes 1976–2009. *Cryosphere*, **4**(2), 429–467 (doi:10.5194/tc-4-419-2010)
- Bolch T and 10 others (2012) The state and fate of Himalayan glaciers. *Science*, **336**(6079), 310–314 (doi: 10.1126/science.1215828)
- Braithwaite RJ and Raper SCB (2009) Estimating equilibrium-line altitude (ELA) from glacier inventory data. *Ann. Glaciol.*, **50**(53), 127–132 (doi: 10.3189/172756410790595930)
- Curry JA and Webster PJ (1999) *Thermodynamics of atmospheres and oceans*. Academic Press, San Diego, CA
- Dadic R, Corripio JG and Burlando P (2008) Mass-balance estimates for Haut Glacier d'Arolla, Switzerland, from 2000 to 2006 using DEMs and distributed mass-balance modeling. *Ann. Glaciol.*, **49**(1), 22–26 (doi: 10.3189/172756408787814816)
- Dong Z, Qin D, Ren J, Li K and Li Z (2012) [Variations in the equilibrium line altitude of Urumqi Glacier No. 1, Tianshan Mountains, over the past 50 years]. *Chinese Sci. Bull.*, **57**(36), 4776–4783 [in Chinese]
- Duguay CR (1993) Radiation modeling in mountainous terrain: review and status. *Mt. Res. Dev.*, **13**, 339–357 (doi: 10.2307/3673761)
- Evans IS and Cox NJ (2005) Global variations of local asymmetry in glacier altitude: separation of north–south and east–west components. *J. Glaciol.*, **51**(174), 469–482 (doi: 10.3189/172756505781829205)
- Fujita K (2008) Effect of precipitation seasonality on climatic sensitivity of glacier mass balance. *Earth Planet. Sci. Lett.*, **276**(1–2), 14–19 (doi: 10.1016/j.epsl.2008.08.028)
- Fujita K and Ageta Y (2000) Effect of summer accumulation on glacier mass balance on the Tibetan Plateau revealed by mass-balance model. *J. Glaciol.*, **46**(153), 244–252 (doi: 10.3189/172756500781832945)
- Fujita K and Nuimura T (2011) Spatially heterogeneous wastage of Himalayan glaciers. *Proc. Natl Acad. Sci. USA (PNAS)*, **108**(34), 14 011–14 014 (doi: 10.1073/pnas.1106242108)
- Gardelle J, Berthier E and Arnaud Y (2012) Slight mass gain of Karakoram glaciers in the early twenty-first century. *Nature Geosci.*, **5**, 322–325 (doi: 10.1038/ngeo1450)
- Giesen RH, Van den Broeke MR, Oerlemans J and Andreassen LM (2008) The surface energy balance in the ablation zone of Middalsbreen, a glacier in southern Norway: interannual variability and the effect of clouds. *J. Geophys. Res.*, **113**(D21), D21111 (doi: 10.1029/2008JD010390)
- Greuell W, Knap WH and Smeets PC (1997) Elevational changes in meteorological variables along a midlatitude glacier during summer. *J. Geophys. Res.*, **102**(D22), 25 941–25 954
- Guo X and 7 others (2011) Critical evaluation of scalar roughness length parametrizations over a melting valley glacier. *Bound.-Layer Meteorol.*, **139**(2), 307–332 (doi: 10.1007/s10546-010-9586-9)
- He J and Yang K (2011) *China Meteorological Forcing Dataset*. Cold and Arid Regions Science Data Center, Lanzhou (doi: 10.3972/westdc.002.2014.d)
- Heynen M, Pellicciotti F and Carenzo M (2013) Parameter sensitivity of a distributed enhanced temperature-index melt model. *Ann. Glaciol.*, **54**(63), 311–321 (doi: http://dx.doi.org/10.3189/2013AoG63A537)
- Hock R and Holmgren B (2005) A distributed surface energy-balance model for complex topography and its application to Storglaciären, Sweden. *J. Glaciol.*, **51**(172), 25–36 (doi: 10.3189/172756505781829566)
- Jacob T, Wahr J, Pfeffer WT and Swenson S (2012) Recent contributions of glaciers and ice caps to sea level rise. *Nature*, **482**(7386), 514–518 (doi:10.1038/nature10847)
- Jiang X, Wang N, Yang S, He J and Song G (2010) [The surface energy balance on the Qiyi Glacier in Qilian Mountains during the ablation period]. *J. Glaciol. Geocryol.* **32**(4), 686–695 [in Chinese]
- Kääb A, Berthier E, Nuth C, Gardelle J and Arnaud Y (2012) Contrasting patterns of early twenty-first-century glacier mass change in the Himalayas. *Nature*, **488**(7412), 495–498 (doi:10.1038/nature11324)
- Kang E and Ohmura A (1994) [A parameterized energy balance model of glacier melting on the Tianshan Mountain]. *Acta Geogr. Sin.*, **49**(5), 467–476 [in Chinese]
- Kang X and Ding L (1981) [Relation of mass balance, ELA and climate in Tianshan Mountain and Qilian Mountain]. *J. Glaciol. Geocryol.*, **3**(1), 53–56 [in Chinese]
- Kayastha RB, Ohata T and Ageta Y (1999) Application of a mass-balance model to a Himalayan glacier. *J. Glaciol.*, **45**(151), 559–567
- Klok E and Oerlemans J (2002) Model study of the spatial distribution of the energy and mass balance of Morteratschgletscher, Switzerland. *J. Glaciol.*, **48**(163), 505–518 (doi: 10.3189/172756502781831133)
- Li J, Liu S and Zhang Y (2007) [Snow surface energy balance over the ablation period on the Keqicar Baxi Glacier in the Tianshan Mountains]. *J. Glaciol. Geocryol.*, **29**(3), 366–373 [in Chinese]
- Ma Y, Zhang Y, Yang D and Farhan SB (2014) Precipitation bias variability versus various gauges under different climatic conditions over the Third Pole Environment (TPE) region. *Int. J. Climatol.* (doi: 10.1002/joc.4045)
- Machguth H, Purves RS, Oerlemans J, Hoelzle M and Paul F (2008) Exploring uncertainty in glacier mass balance modelling with Monte Carlo simulation. *Cryosphere*, **2**(2), 191–204 (doi:10.5194/tc-2-191-2008)
- Maussion F and 9 others (2011) Glaciological field studies at Zhadang Glacier (5500–6095 m), Tibetan Plateau. In *Workshop on the use of automatic measuring systems on glaciers. IASC Workshop, 23–26 March 2011, Pontresina (Switzerland)*. Institute for Marine and Atmospheric Research, Utrecht University, Utrecht, 62–68 <http://www.projects.science.uu.nl/iceclimate/workshop/documents/abstracts2011.pdf>
- Maussion F, Scherer D, Mölg T, Collier E, Curio J and Finkelnburg R (2014) Precipitation seasonality and variability over the Tibetan Plateau as resolved by the High Asia Reanalysis. *J. Climate*, **27**, 1910–1927 (doi: 10.1175/JCLI-D-13-00282.1)
- Mölg T and Hardy DR (2004) Ablation and associated energy balance of a horizontal glacier surface on Kilimanjaro. *J. Geophys. Res.*, **109**(D16), D16104 (doi: 10.1029/2003JD004338)
- Mölg T, Cullen NJ, Hardy DR, Kaser G and Klok L (2008) Mass balance of a slope glacier on Kilimanjaro and its sensitivity to climate. *Int. J. Climatol.*, **28**(7), 881–892 (doi: 10.1002/joc.1589)
- Mölg T, Maussion F, Yang W and Scherer D (2012) The footprint of Asian monsoon dynamics in the mass and energy balance of a Tibetan glacier. *Cryosphere*, **6**, 1445–1461 (doi:10.5194/tc-6-1445-2012)
- Mölg T, Maussion F and Scherer D (2014) Mid-latitude westerlies as a driver of glacier variability in monsoonal High Asia. *Nature Climate Change*, **4**, 68–73 (doi: 10.1038/NCLIMATE2055)
- Oerlemans J, Giesen RH and Van den Broeke MR (2009) Retreating alpine glaciers: increased melt rates due to accumulation of dust

- (Vadret da Morteratsch, Switzerland). *J. Glaciol.*, **55**(192), 729–736 (doi: 10.3189/002214309789470969)
- Pellicciotti F and 7 others (2008) A study of the energy balance and melt regime on Juncal Norte Glacier, semi-arid Andes of central Chile, using melt models of different complexity. *Hydrol. Process.*, **22**(19), 3980–3997 (doi: 10.1002/hyp.7085)
- Pu J, Yao T, Zhang Y, Seko K and Fujita K (1995) [Mass balance on the Dongkemadi and Meikuang Glaciers in 1992/1993]. *J. Glaciol. Geocryol.*, **17**(2), 138–142 [in Chinese]
- Reijmer CH and Hock R (2008) Internal accumulation on Storglaciaren, Sweden, in a multi-layer snow model coupled to a distributed energy- and mass-balance model. *J. Glaciol.*, **54**(184), 61–72 (doi: 10.3189/002214308784409161)
- Rupper S and Roe G (2008) Glacier changes and regional climate: a mass and energy balance approach. *J. Climate*, **21**(20), 5384–5401 (doi: 10.1175/2008JCLI2219.1)
- Scherler D, Bookhagen B and Strecker MR (2011) Spatially variable response of Himalayan glaciers to climate change affected by debris cover. *Nature Geosci.*, **4**, 156–159 (doi: 10.1038/NNGEO103101068)
- Shi Y and Liu S (2000) [Estimation on the response of glaciers in China to the global warming in the 21st century]. *Chinese Sci. Bull.*, **45**(7), 668–672 (doi: 10.1007/BF02886048) [in Chinese]
- Shi Y, Liu C, Wang Z, Liu S and Ye B (2005) [A concise China glacier inventory]. Shanghai Science Popularization Press, Shanghai [in Chinese]
- Sicart JE, Hock R, Ribstein P and Chazarin JP (2010) Sky longwave radiation on tropical Andean glaciers: parameterization and sensitivity to atmospheric variables. *J. Glaciol.*, **56**(199), 854–860 (doi: 10.3189/002214310794457182)
- Smeets CJPP (2006) Assessing unspirated temperature measurements using a thermocouple and a physically based model. In *The Mass Budget of Arctic Glaciers. Extended abstracts – Workshop and GLACIODYN Planning Meeting 2006*. Institute for Marine and Atmospheric Research, Utrecht, 99–101
- Strasser U, Corripio J, Pellicciotti F, Burlando P, Brock B and Funk M (2004) Spatial and temporal variability of meteorological variables at Haut Glacier d'Arolla (Switzerland) during the ablation season 2001: measurements and simulations. *J. Geophys. Res.*, **109**(D3), D03103 (doi: 10.1029/2003JD003973)
- Sun W and 7 others (2012) The surface energy budget in the accumulation zone of the Laohugou Glacier No. 12 in the Western Qilian Mountains, China, in summer 2009. *Arct. Antarct. Alp. Res.*, **44**(3), 296–305 (doi: 10.1657/1938-4246-44.3.296)
- Takahashi S, Ohata T and Xie Y (1989) Characteristics of heat and water fluxes on glacier and ground surfaces in the West Kunlun Mountains. *Bull. Glacier Res.*, **7**, 89–98
- Van den Broeke MR, Smeets P, Ettema J, Van der Veen C, Van de Wal R and Oerlemans J (2008) Partitioning of melt energy and meltwater fluxes in the ablation zone of the west Greenland ice sheet. *Cryosphere*, **2**, 179–189 (doi:10.5194/tc-2-179-2008)
- Wagnon P and 11 others (2013) Seasonal and annual mass balances of Mera and Pokalde glaciers (Nepal Himalaya) since 2007. *Cryosphere*, **7**(6), 1769–1786 (doi: 10.5194/tc-7-1769-2013)
- Wang N, He J, Pu J, Jiang X and Jing Z (2010) [Variations in equilibrium line altitude of the Qiyi Glacier, Qilian Mountains, over the past 50 years]. *Chinese Sci. Bull.*, **55**(33), 3810–3817 [in Chinese]
- Wang Z, Deng Y and Zeng X (1982) [Water-heat conditions for maritime glaciers developing in Guxiang, Tibetan Region]. In *Memoirs of Lanzhou Institute of Glaciology and Geocryology, CAS, No. 3*. Science Press, Beijing, 82–90 [in Chinese]
- Xie Y (1994) [Autumn heat balance in the ablation area of Hailuogou Glacier]. In Xie Z and Kotlyakov VM eds *Glaciers and environment in the Tibet Plateau (1), the Gongga Mountain*. Science Press, Beijing, 94–109 [in Chinese]
- Yang D and 6 others (1998) Accuracy of NWS 8-inch standard nonrecording precipitation gauge: results and application of WMO intercomparison. *J. Atmos. Ocean. Technol.*, **15**(1), 54–68
- Yang K, He J, Tang W, Qin J and Cheng CCK (2010) On downward shortwave and longwave radiations over high altitude regions: observation and modeling in the Tibetan Plateau. *Agric. Forest Meteorol.*, **150**(1), 38–46 (doi: 10.1016/j.agrformet.2009.08.004)
- Yang W and 6 others (2011) Summertime surface energy budget and ablation modeling in the ablation zone of a maritime Tibetan glacier. *J. Geophys. Res.*, **116**(D14), D14116 (doi: 10.1029/2010JD015183)
- Yang W, Yao T, Guo X, Zhu M, Li S and Kattel DB (2013) Mass balance of a maritime glacier on the southeast Tibetan Plateau and its climatic sensitivity. *J. Geophys. Res.*, **118**, 1–16 (doi: 10.1002/jgrd.50760)
- Yao T and 7 others (2010) [Glacial distribution and mass balance in the Yarlung Zangbo River and its influence on lakes]. *Chinese Sci. Bull.*, **55**(20), 2072–2078 [in Chinese]
- Yao T and 14 others (2012) Different glacier status with atmospheric circulations in Tibetan Plateau and surroundings. *Nature Climate Change*, **2**, 663–667 (doi: 10.1038/nclimate1580)
- Yu W and 10 others (2013) Different region climate regimes and topography affect the changes in area and mass balance of glaciers on the north and south slopes of the same glacierized massif (the West Nyainqentanglha Range, Tibetan Plateau). *J. Hydrol.*, **495**, 64–73 (doi:10.1016/j.jhydrol.2013.04.034)
- Zhang G and 9 others (2013) Energy and mass balance of Zhadang glacier surface, central Tibetan Plateau. *J. Glaciol.*, **59**(213), 137–148 (doi: 10.3189/2013JoG12J152)
- Zhang Y and Liu S (2006) [Preliminary study of mass balance on the Keqicar Baxi Glacier on the south slopes of Tianshan Mountains]. *J. Glaciol. Geocryol.*, **28**(4), 477–484 [in Chinese]
- Zhang Y, Yao T, Pu J, Ohata T, Yabuki H and Fujita K (1996) [Energy budget at ELA on Dongkemadi Glacier in the Tanggula Mountains, Tibetan Plateau]. *J. Glaciol. Geocryol.*, **18**(1), 10–19 [in Chinese with English summary]
- Zhang Y, Fujita K, Ageta Y, Nakawo M, Yao T and Pu J (1998) The response of glacier ELA to climate fluctuations on High-Asia. *Bull. Glacier Res.*, **16**, 1–11
- Zhou S, Kang S, Gao T and Zhang G (2010) Response of Zhadang Glacier runoff in Nam Co Basin, Tibet, to changes in air temperature and precipitation form. *Chinese Sci. Bull.*, **55**(20), 2103–2110

APPENDIX: DESCRIPTION OF PARAMETERS AND FORMULAS IN THE ENERGY- AND MASS-BALANCE MODEL

Albedo (α) is parameterized for both glaciers, as in Yang and others (2013) on Parlung No. 94 glacier and Mölg and others (2012) on Zhadang glacier. The ice surface albedo was assumed to vary as a function of the dew-point temperature (Mölg and others, 2008):

$$\alpha_{\text{ice}} = aT_c + b \quad (\text{A1})$$

$$\alpha_s^{(i)} = \alpha_{\text{firm}} + (\alpha_{\text{freshsnow}} - \alpha_{\text{firm}}) \exp\left(\frac{s-i}{t^*}\right) \quad (\text{A2})$$

$$\alpha^{(i)} = \alpha_s^{(i)} + (\alpha_{\text{ice}} - \alpha_s^{(i)}) \exp\left(\frac{-d}{d^*}\right) \quad (\text{A3})$$

where α_{ice} is ice surface albedo, a and b are the two constants, T_c is dew-point temperature, α_s is the albedo of snow, which is calculated using Eqn (A2), α_{firm} is the firm albedo, $\alpha_{\text{freshsnow}}$ is the fresh-snow albedo, s is the time since the last snowfall event (days), i is the actual time, t^* is timescale, d is the snow depth (cm) and d^* is the characteristic scale for snow depth. Given that the relatively thin fresh snowpack likely melted away within a few hours in summer, a snowfall threshold (Z_{th}) was introduced to determine whether fresh snowfall could persist through an

Table 5. Input parameters for the energy- and mass-balance model on Zhadang and Parlung No. 4 glaciers

Symbol	Parameter	Value	
		Zhadang	Parlung No. 4
ΔP	Vertical precipitation gradient	0.038 % m ⁻¹	0.25 % m ⁻¹
Z_{th}	Snowfall event threshold	5 cm	3.8 cm
T_{snow}	Phase threshold for snow	1°C	-0.5°C
T_{rain}	Phase threshold for rain	6.5°C	2.3°C
PP_{snow}	Fraction of S_{net} absorbed in snow surface layer	0.075	0.075
PP_{ice}	Fraction of S_{net} absorbed in ice surface layer	0.15	0.113
$\alpha_{freshsnow}$	Fresh snow albedo	0.8	0.85
α_{firn}	Firn albedo	0.6	0.5
t^*	Albedo timescale	6 days	3.11 days
d^*	Albedo depth scale	8 cm	5.743 cm
a	Parameter of ice albedo	-0.0438°C ⁻¹	-0.0313°C ⁻¹
b	Parameter of ice albedo	0.2157	0.2577
C_1	Parameter of L_{in}	0.6586 hPa ⁻¹	0.631 hPa ⁻¹
C_2	Parameter of L_{in}	0.0363 hPa ⁻¹	0.04847 hPa ⁻¹
C_S	Snow exchange coefficient of turbulent heat flux	0.002	0.0038
C_L	Ice exchange coefficient of turbulent heat flux	0.002	0.0038

entire daily cycle. The L_{in} value is calculated according to the air temperature and humidity (Duguay, 1993):

$$L_{in} = \sigma(T + 273.15)^4(C_1 + C_2 e_a) \quad (\text{A4})$$

where T is the air temperature, e_a is the water vapour pressure of the air (hPa) calculated from relative humidity and air temperature, σ is the Stefan–Boltzmann constant ($5.67 \times 10^{-8} \text{ W m}^{-2} \text{ K}^{-4}$) and C_1 and C_2 are empirical constants (Table 5). L_{out} is calculated conventionally by the Stefan–Boltzmann law from modelled surface temperature (T_S) and surface emissivity ($\varepsilon = 1$):

$$L_{out} = \sigma\varepsilon(T_S + 273.15)^4 \quad (\text{A5})$$

The turbulent fluxes are computed using the bulk method based on differences in temperature, humidity and wind speed between the measurement level and the surface.

$$H_{sen} = \rho_{air} C_p u C_S (T - T_S) \quad (\text{A6})$$

$$H_{lat} = \rho_{air} L_V u C_L (q - q_s) \quad (\text{A7})$$

where ρ_{air} is the density of air (kg m^{-3}), C_p is the specific heat of air at constant air pressure ($1006 \text{ J kg}^{-1} \text{ K}^{-1}$), C_S and C_L are constant bulk exchange coefficients used to calculate the turbulent heat flux (Yang and others, 2013; Zhang and others, 2013), u is the wind speed (m s^{-1}) and q and q_s are the specific humidity at 2 m and at the snow/ice surface, respectively.

The total energy flux in the subsurface (QG) consists of a conductive heat flux (G) and an energy flux due to the penetrating shortwave radiation (QPS). The conductive heat flux (G) was computed from the one-dimensional heat-transfer equation for 0.1 m thick layers for snow and 0.5 m layers for ice below snow. Meanwhile, the model classified each layer as snow and ice. The penetrating shortwave radiation (QPS) was calculated as fractions of the net shortwave radiation over snow (PP_{snow}) and ice (PP_{ice}). The values of the extinction coefficient in QPS are taken from Yang and others (2013) on Parlung No. 4 glacier and from Mölg and others (2014) on Zhadang glacier. Using an iterative procedure, the surface energy balance was solved for the surface temperature T_S (Fujita and Ageta, 2000; Yang and others, 2013). If the T_S determined by the model is higher than the melting point temperature, T_S is set back to 0°C, and the excess energy is used for melting.

P_{snow} is modelled by the total daily precipitation P , which is calculated by the vertical precipitation gradient ΔP , and two critical air temperature thresholds for rain (T_{rain}) and snow (T_{snow}). We used linear interpolation to separate the rain and snow from measured precipitation. The T_{snow} and T_{rain} for Zhadang glacier are assumed to be 1°C and 6.5°C (Zhou and others, 2010; Mölg and others, 2012), respectively, and -0.5°C and 2.3°C for Parlung No. 4 glacier (Yang and others, 2013).

MS received 31 October 2014 and accepted in revised form 10 April 2015